AIAA 2003 - 1318

# Analyses of Direct Detonation Initiation with Realistic Finite-Rate Chemistry

Kyoung-Su Im and S.-T. John Yu
Mechanical Engineering Department
Wayne State University, Detroit MI 48202

**41th Aerospace Sciences Meeting & Exhibit**
06 - 09 January 2003
Reno, Nevada

# Analyses of Direct Detonation Initiation with Realistic Finite-Rate Chemistry

**Kyoung-Su Im[1] and S.-T. John Yu[2]**

Mechanical Engineering Department
Wayne State University, Detroit, MI48202

## ABSTRACT

The present paper reports high-fidelity simulation of direct initiation processes of cylindrical detonation waves by concentrated energy deposition. The goal is to understand the underpinning mechanisms in failed or successful detonation initiation processes. We employed the Space-Time CESE method to solve the reacting flow equations, including realistic finite-rate chemistry model of the nine species and twenty-four reactions for $H_2$-$O_2$-Ar mixtures. Detailed results of sub-critical, critical, and supercritical initiation process are reported. Contribution of competing terms in the temperature reaction zone structure equation is analyzed. We found that the unsteadiness terms play the critical role in the initiation process.

## 1. INTRODUCTION

In general, there are three experimental methods to initiate detonation: (i) flame initiation, (ii) shock wave initiation, and (iii) direct initiation. In all three cases, shock waves occur prior to detonation initiation. The present paper focuses on the third initiation mode, which is relevant to the detonation initiation process in a PDE. For background information, a brief account of the above three initiation modes is provided in the following.

In the flame initiation mode [7], a weak spark ignites an explosive gas mixture, which is usually confided in an enclosure. The generated flame propagates towards the unburned gas mixture because hotter burned gas has higher specific volume than that of the unburned gas. The flow motion acts like a hot-gas piston and generates a compression wave, which imparts a downstream velocity to the unburned gases ahead of the flame. Under suitable conditions, traveling compression waves will produce a shock wave ahead of the flame. With enough transition distance, the accelerating flame will be strengthened and catch up the shock. As a result, a detonation is initiated. Two possible mechanisms are responsible for flame acceleration: (i) increasing flame area that increases heat release rate, and (ii) induced turbulence in the moving unburned mixture ahead of the flame which allow the flame to leap ahead. This process is referred to as deflagration to detonation transition (DDT) or self-initiation because the detonation is initiated solely by the energy release from the combustion of the mixture itself. The most important parameter in this process is the run-up distance, which depends on the tube geometry, igniter location, and the thermodynamic conditions of the mixtures.

In the shock initiation mode [2], either an incident or reflected shock wave is the primarily means to produce the detonation. The shock rapidly heats the gas by compression. Under suitable conditions, an adiabatic explosion occurs behind the shock wave. This explosion generates accelerating pressure waves, which quickly become a detonation wave itself before catching up with the initially applied shock wave. Upon catching up the leading shock wave, a new and stronger detonation wave occurs.

In the direct initiation mode [1, 3], a large amount of energy is instantaneously deposited to a small region of unconfined combustible mixture. Immediately, a strong blast wave is generated. This spherical (or cylindrical) shock wave expands and decays while it continues heating the gas mixture. Due to shock heating, chemical reactions occur and chemical energy is released. Under

[1] Research Assistant Professor, AIAA member, Email: ksim@fluid.eng.wayne.edu
[2] Associate Professor, AIAA member, Email: styu@me1.eng.wayne.edu

suitable conditions, detonation is initiated. The blast wave generated by igniter plays an important role because it produces the critical states for the onset of the detonation. Therefore, it is often referred to as the blast initiation.

Zeldovich et al. [1] studied the direct detonation initiation process by sparks. They pointed out that the amount of the deposited energy, or the critical energy, is the key parameter controlling the initiation process. Later on, Bach et al. [3] summarized theoretical and experimental studies of spherical detonation waves initiated by a laser-induced spark. They classified the three different regimes of the initiation processes according to the magnitude of the initiation energy: (i) the supercritical regime for successful detonation initiation, (ii) the sub-critical regime for failed initiation, and (iii) the critical regime for marginally sustainable detonation initiation.

Many attempts have been made to predict the critical energy for initiating detonation under various circumstances. He and Clavin [4, 6] performed quasi-steady analysis of the direct initiation process. They developed the critical curvature model, which states that the failure mechanism of the detonation is mainly caused by the nonlinear curvature effect of the wave front. Eckett and Shepherd [11] proposed the critical decay rate model, in which they pointed out that the critical mechanism of a failed detonation initiation is due to the unsteadiness of the reacting flow. Their theory for spherical detonation initiation has been supported by numerical simulation and experimental data.

Due to simplicity and computational efficiency, numerical analyses for the detonation initiation have been based on the use of (i) single-step irreversible reaction models, and (ii) the assumption of a polytropic gas mixture. However, in a recent numerical study, Mazaheri [8] showed that with a single-step model, critical initiation energy does not exist because the decaying blast wave always becomes a detonation in its development. In order to catch the essential features of real detonation initiation phenomena, Lee and Higgins [9] strongly suggested that one should abandon the single-step chemistry model and adopt real finite rate chemistry models and thermodynamics calculations.

In this paper, we focus on direct initiation of cylindrical detonation in an $H_2/O_2/Ar$ mixture. A finite-rate model of twenty-four reaction steps and nine species is adopted. Various values of initiation energy are used to simulate the supercritical, the sub-critical, and the critical processes. We analyzed the numerical solutions in the reaction zone to study the underpinning physics in the direct initiation processes. The rest of the paper is organized as follows. Section 2 shows the model equations. Section 3 reports the results and discussions. We then offer concluding remarks and provide the cited references.

## 2. MODEL EQUATIONS

### 2.1 Reacting Flow Equations

The governing equations for the numerical simulation are the one-dimensional multi-species reactive Euler equations of $N_s$ species:

$$\frac{\partial \mathbf{U}}{\partial t} + \frac{\partial \mathbf{F}(\mathbf{U})}{\partial r} = \mathbf{G}(\mathbf{U}) + \mathbf{S}(\mathbf{U}) \tag{2.1}$$

where

$$\begin{aligned}
\mathbf{U} &= (\rho, \rho u, \rho E, \rho_1, \rho_2, \ldots, \rho_{N_s-1})^{\mathrm{T}} \\
\mathbf{F} &= (\rho u, \rho u^2 + p, (\rho E + p)u, \rho_1 u, \rho_2 u, \ldots, \rho_{N_s-1} u)^{\mathrm{T}} \\
\mathbf{G} &= -\frac{j}{r}\left(\rho u, \rho u^2, (\rho E + p)u, \rho_1 u, \rho_2, \ldots, \rho_{N_s-1} u\right)^{\mathrm{T}} \\
\mathbf{S} &= \left(0, 0, 0, \dot{w}_1, \dot{w}_2, \ldots, \dot{w}_{N_s-1}\right)^{\mathrm{T}}
\end{aligned} \tag{2.2}$$

$\rho$, $u$, $p$, $E$, and $\rho_k$ are density, velocity, specific total energy, and mass concentration of species $k$, respectively. $j = 0, 1, 2$ for planar, cylindrical, and spherical flows, respectively. $\rho$ is the summation of all species density,

$$\rho = \sum_{k=1}^{Ns} \rho_k \tag{2.3}$$

The total energy $E$ is defined as

$$E = e + u^2 / 2 \tag{2.4}$$

where $e$ is the internal energy of the gas mixture per unit mass and it is calculated based on a mass-weighted average of the specific internal energy of each species $e_k$, i.e.,

$$e = \sum_{k=1}^{Ns} y_k e_k \tag{2.5}$$

In Eq. (2.5), $y_k = \rho_k / \rho$ is the mass fraction of species $k$. Note that since the internal energy $e$ and the total energy $E$ include the heat of formation of each species in their definitions, no source term exists in the energy equation.

$\dot{w}_k$ is the net molar production rate of species $k$ and can also be expressed as $\dot{w}_k = \rho W_k / W_k$

According to the law of mass action, the stoichiometric equation of a set of $N_r$ elementary reactions involving $N_s$ species can be written in the following form

$$\sum_{k=1}^{N_s} n'_{jk} n_k \underset{K_{bj}}{\overset{K_{fj}}{\Leftrightarrow}} \sum_{k=1}^{N_s} n''_{jk} n_k, \quad j = 1,2,\ldots,N_r \qquad (2.6)$$

where $n_k = r_k / W_k$ is the mole concentration of species $k$ in the gas mixture. $n'_{jk}$ and $n''_{jk}$ are respectively the stoichiometric coefficients of the reactants and products of species $k$ in the $j$th reaction. The source terms, $\dot{w}_k$ for $k=1,2,3,..,N_{s-1}$, in the species equations, Eq. (2.2), are formulated in mass concentration, and they are the summation of the net rate of change of species $k$ from all chemical reactions involved, i.e.,

$$\dot{w}_k = W_k \sum_{j=1}^{N_r} (\dot{n}_k)_j \qquad (2.7)$$

where $W_k$ is the molecular weight of species and $(\dot{n}_k)_j$ is the rate change of concentration of species $k$ by the reaction $j$, given by

$$(\dot{n}_k)_j = (n''_{jk} - n'_{jk}) \left( K_{f_j} \prod_{l=1}^{N_s} n_l^{n'_{jl}} - K_{b_j} \prod_{l=1}^{N_s} n_l^{n''_{jl}} \right) \qquad (2.8)$$

The forward and backward reaction rate constants, $K_{fj}$ and $K_{bj}$, are in the Arrhenius form:

$$\begin{aligned} K_{f_j} &= A_{f_j} T^{B_{f_j}} \exp\left(-E_{f_j} / R_u T\right) \\ K_{b_j} &= A_{b_j} T^{B_{b_j}} \exp\left(-E_{b_j} / R_u T\right) \end{aligned} \qquad (2.9)$$

where $A_f$ and $A_b$ are the pre-exponential constant; $E_f$ and $E_b$ are the activation energies; and $R_u$ is the universal gas constant. In general, those coefficients in Eq. (2.9) are provided as a part of the adopted finite-rate chemistry model. If the kinetic data of the reverse reaction were not available, one needs to use the equilibrium constant to calculate the reverse reaction rate constants, i.e.,

$$K_{b_j} = K_{f_j} / K_{eq_j} \qquad (2.10)$$

where the $K_{eqj}$ is determined by minimizing the free energy [11].

### 2.2 Initial and Boundary Conditions

The initial conditions are taken from reference [6]. A specific amount of energy, $E_s$, in the form of high temperature and high pressure (with a subscript $s$) is deposited instantaneously into the driver section of a reactive gas mixture. On the other hand, low temperature and pressure are set for the driven section.

$$\begin{aligned} &\text{If } 0 \le r < r_s, \quad p = p_s, T = T_s, y_i = y_s, u = u_s, \\ &\qquad r \ge r_s, \quad p = p_0, T = T_0, y_i = y_i, u = u_0 \end{aligned} \qquad (2.11)$$

Refer to Figure 2.1. The radius of the driver section $r_s$ is about 15 times smaller than the critical radius $R_c$ [6]. Inside the driver section, pressure is set about 15-20 times higher than the peak values of the corresponding C-J detonation. Essentially, the initial condition provides a strong cylindrical expanding blast wave to be expanded in the radial direction. The species compositions at both sides are $H_2+O_2+7Ar$. The pressure and temperature of the driven section are 0.2 atm and 298K, respectively. The deposited energy $E_s$ is calculated based on the internal energy equation for a perfect gas:

$$\begin{aligned} &E_s = s_j r_s^{j+1} p_s / (g-1) \\ &\text{and} \\ &\qquad s_j = [2jp + (j-1)(j-2)] / (j+1) \end{aligned} \qquad (2.12)$$

Several values of $E_s$ are selected in the present calculations: $E_s$ = *33.9*, *43.0*, *53.0*, and *76.3 J/cm*, corresponding to the initiation radius $r_s$ = 0.4, 0.45, 0.5, and *0.6 cm*, respectively. Pressure at the driver section, $p_s$, is set *200* atm for all calculations.

Two boundary conditions are used in the calculation. At $r=0$, the boundary conditions are derived based on a limiting form of Eqn. (2.2) when $r$ approaching null. At $r=¥$, the standard non-reflecting boundary conditions are employed.

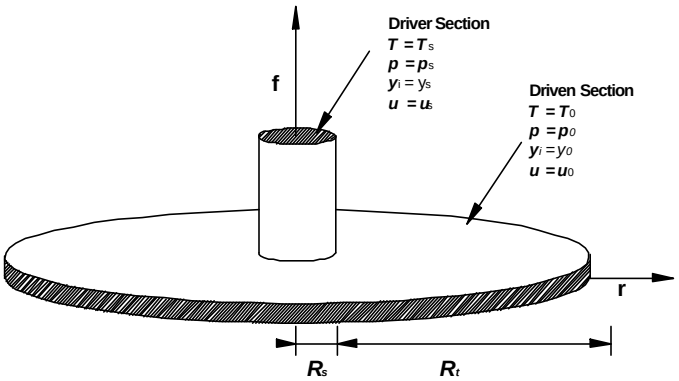


Fig. 2.1: A schematic of the initial condition of the direct detonation initiation process.

## 3. NUMERICAL METHOD

The space-time Conservation Element Solution Element (CESE) method, originally proposed by Chang [5] has been extended for chemical reacting flows with

realistic finite-rate chemistry models. The CESE method is distinguished by the simplicity of its design principle, i.e., treating space and time as one entity in calculating flux conservation. Previously, we have reported the extension of the CESE method for chemically reacting flows with comprehensive physical modeling, including the multi-step finite-rate kinetics and thermodynamics models [10, 12]

## 4. REACTION ZONE EUQATIONS

In reference [11], the reaction zone equations are derived based on one-dimensional reactive Euler equations in the shock reference frame. The following relations are used to transform the equations in the lab frame to the shock frame:

$$x = R(t) - r$$
$$w(x,t) = U(t) - u(r,t)$$

where $R$ and $U$ are the position and velocity of the shock in the lab frame, and $w$ is the flow velocity in the shock frame.

The equations for velocity, density and pressure along a Lagrangian particle path behind the shock are given by

$$h\frac{Dw}{Dt} = w\dot{s} - \frac{j}{R-x}w(U-w) - M^2\frac{dU}{dt} + \frac{\partial w}{\partial t} - \frac{w}{rc^2}\frac{\partial P}{\partial t} \quad (4.1)$$

$$h\frac{Dr}{Dt} = -r\dot{s} - \frac{j}{R-x}rM^2(U-w) + \frac{rw}{c^2}\frac{dU}{dt} - \frac{rw}{c^2}\frac{\partial w}{\partial t} + \frac{1}{c^2}\frac{\partial P}{\partial t} \quad (4.2)$$

$$h\frac{DP}{Dt} = -rw^2\dot{s} - \frac{j}{R-x}rw^2(U-w) + rw\frac{dU}{dt} - ?? \frac{\partial w}{\partial t} + \frac{\partial P}{\partial t} \quad (4.3)$$

where $r$ and $P$ are density and pressure, and $t$ is time. $j$ = 0 for planar, 1 for cylindrically symmetric and 2 for spherically symmetric. The Mach number $M$ and sonic parameter $h$ are given by

$$M = \frac{w}{c},\ h = 1 - M^2$$

where $c$ is the frozen sound speed, $\dot{s} = \sum s_k W_k$ is the total thermicity, and $s_k$ is the thermicity coefficient of species $k$:

$$s_k = \frac{1}{rc^2}\frac{\partial P}{\partial y_k}\bigg|_{e,r,y_{j\neq k}} = -\frac{1}{rc^2}\frac{(\partial e/\partial y_k)|_{P,r,y_{j\neq k}}}{(\partial e/\partial P)|_{r,y}} \quad (4.4)$$

where $y_k$ is the mass fraction of species $k$, and $W_k$ is the production rate of species $k$, provided by the adopted chemistry model.

When the detonation wave propagates into the reactant mixture, a sharp temperature increase occurs. If the flow particles followed the sharp temperature gradient closely, the detonation will be sustained. The chemical reaction rate depends on the temperature. Thus temperature of the flow particle in the vicinity of the reaction zone becomes the most important parameter in determining failure or success of the detonation initiation process. The derivation of the temperature equation in the reaction zone can be found in [11]:

$$hC_p\frac{DT}{Dt} = -(1-gM^2)\sum e_k W_k - \frac{c^2}{g}\sum\frac{W}{W_k}W_k + \frac{j}{R-x}w^2(U-w) + w\frac{dU}{dt} - w\frac{\partial w}{\partial t} + \frac{1}{r}\frac{\partial P}{\partial t} \quad (4.5)$$

where $e_k$ is the specific internal energy of species $k$, $C_p$ is the mixture specific heat at constant pressure, $W$ is the mean molar mass of the mixture, and $W_k$ is the molar mass of species $k$.

In Eqs. (4.1-3, 5), the left-hand side is the total derivative term. The first term on the right-hand side is for the chemical heat release, the second term is due to curvature, and the remaining terms are the unsteadiness terms. Note that with only heat release term, the equations are for the classical ZND solution of a planar detonation wave.

In [11], Eckett, Quirk, and Shepherd compared the magnitude of each term in Eqn. (4.5) to determine the physical processes of the detonation initiation. In the present paper, we conducted similar studies based on numerical results of realistic finite-rate chemistry models. The goal here is to identify the dominant term among the competing terms in Eqn. (4.5) via numerical simulation.

## 5. RESULTS AND DISCUSSION

Bach, Knystautas, and Lee [3] found three propagation regimes direct initiation process, i.e., the sub-critical, the critical, and the supercritical regimes.

In the sub-critical regime, if the deposited initiation energy is below the critical value, the reaction front is always decoupled from the leading shock wave. As a

result, the blast wave eventually decays to an acoustic wave and no detonation occurs.

In the critical regime, the deposited energy is very close to the critical value. At the initial stage of the wave development, the overdriven detonation continuously decays. Then, for a certain short period, the shock wave and the reaction front propagate at a quasi-steady mode, propagating at almost constant shock velocity. Suddenly, local explosions occur at isolated spots in reaction zone, and a detonation wave is developed.

In the supercritical regime, the initiation energy greatly exceeds the critical value. The shock wave is always attached to the reaction front. The overdriven detonation decays continuously to become a self–sustained CJ detonation.

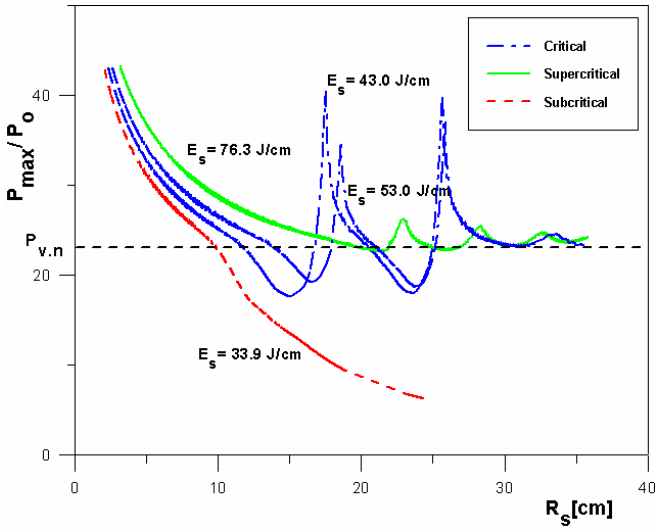


Fig. 5.1: The spatial histories of local maximum pressures in the three regimes of direct initiation processes of a cylindrical detonation in a $H_2 + O_2 + 7Ar$ mixture.

Fig. 5.1 shows the numerical simulation of three regimes of direct initiation according to different initiation energy. The ratio of local maximum pressure to initial reactant pressure is plotted as a function of the radial locations of the leading shock wave. For reference, the pressure of the von-Neuman spike of the corresponding self sustained CJ detonation (for the driven section) is also plotted by dot line. In a series of calculations by incrementally increasing the values of the deposited initiation energy, we can clearly observe the three regimes.

When the initial energy $E_s$ = 33.0 *J/cm*, the strong blast wave decays to a wave with peak pressures much lower than the CJ value, indicating a failed detonation initiation process. Two initial energies of $E_s$ = *43.0 J/cm* and $E_s$ = 53.0 *J/cm* are in the critical regime. Distinct pressure peaks are observed. The deposited initiation energies are not high enough to sustain stable detonation waves. This unstable period ends at *R = 30cm*, and the waves become the self–sustained CJ detonation waves. With higher initiation energy for $E_s$ = *76.3 J/cm*, the initial blast wave directly initiate the detonation wave, which expands and decays to the CJ value with mild instabilities.

Figure 5.2 shows the spatial pressure profiles for $E_s$ = *33.0 J/cm* and $E_s$ = *43.0 J/cm*. In Fig. 5.2(a), initially, strong pressure continuously decays to be below the von Neumann pressure. At *R = 13 cm*, the shock wave is decoupled from the reaction front. After this separation, chemical reaction disappears and the detonation initiation fails.

In Fig. 5.2(b), the initial development of the reactive wave is similar to that of Fig. 5.1(a). However, at *R= 16 cm*, pressure pulse occurs in the reaction zone, and the reactive wave becomes unstable overdriven detonation. Intermittently, the pressure peaks of this overdriven detonation wave decay to sub CJ values. As time evolves, it gradually converges to the CJ detonation, indicating a successful initiation process. It is interesting to note that the instability in the initiation process with repeated pressure peaks, is quite different from the previous results reported in [8, 10], in which the calculations were based on the use of irreversible single step chemistry model.

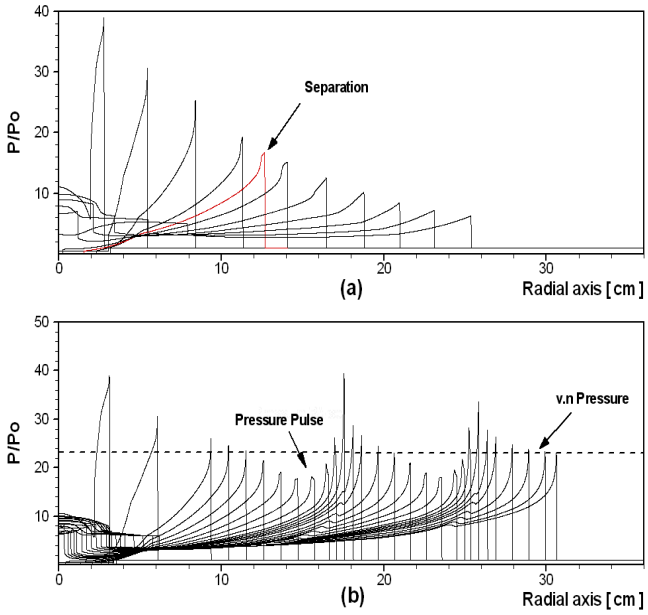


Fig. 5.2: Spatial pressure profiles for the failed and successful initiation processes. (a) $E_s$ = *33.9 J/cm*, and (b) $E_s$ = *43.0 J/cm*.

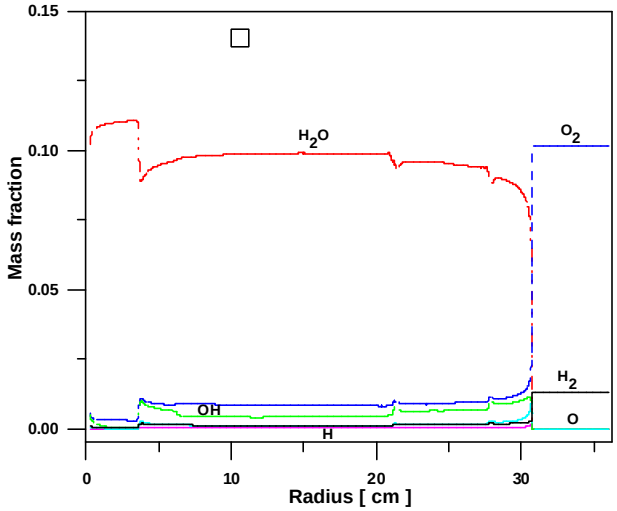


Fig. 5.3: Snapshot of species mass fractions at time t = 192.3 μs in a successful detonation initiation process.

Figure 5.3 shows mass fractions of chemical species at time *t = 192.3 ms*. The mass fractions of all species change rapidly inside the reaction zone. We note that the determination of the reaction zone is not straightforward since the end of the reaction zone is somewhat arbitrary. In the present calculation, the reaction zone is determined by the mass fraction of $H_2O$ since it varies from 0 to some maximum value in combustion process.

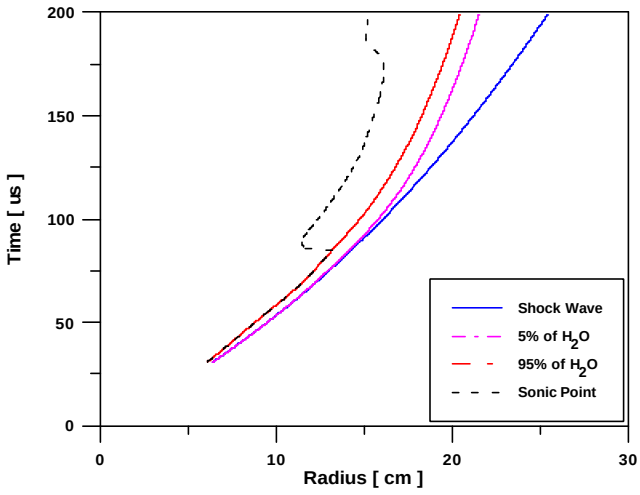


(a)

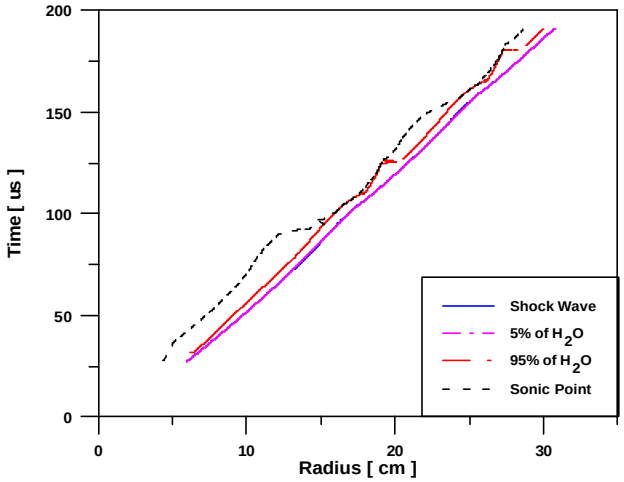


(b)

Fig. 5.4: Evolving reaction zone versus time for (a) a failed, and (b) a successful initiation processes.

The position of the leading shock, the loci of 5% and 95% mass fraction of $H_2O$ species, and the sonic surface are plotted against the elapsed time in Fig. 5.4 to show the development of the reaction zone. The results here are corresponding to that of Fig. 5.2. In Fig. 5.4(a), at the initial stage when shock is strong, the reaction front is attached to the shock wave. At around *R = 13 cm*, the reaction zone begins to detach from the shock wave, indicating that the detonation has failed and the reaction has quenched. In Fig. 5.4(b), the reaction front is continuously coupled with the shock wave, indicating successful initiation of a detonation.

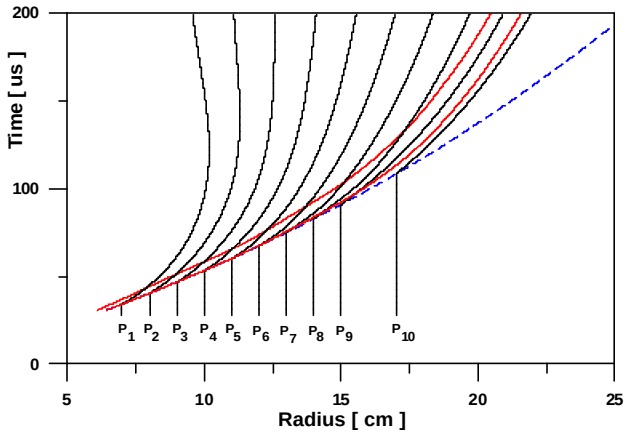


Fig. 5.5: Particle paths in a failed initiation process with $E_s$ = *33.9 J/cm*.

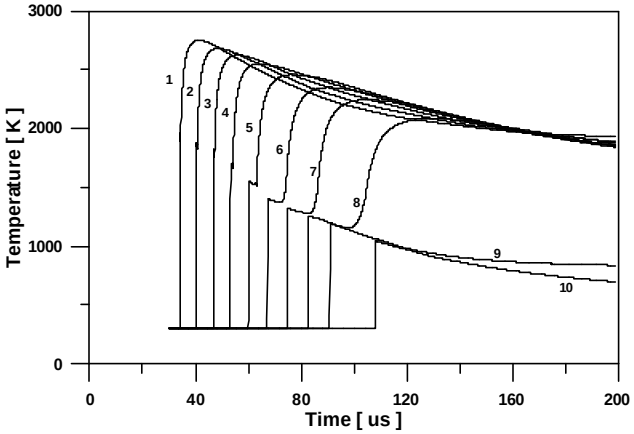


Fig. 5.6: Temperature histories of fluid particle paths for $E_s = 33.9$ *J/cm*.

In the near-critical region, i.e., $E_s = 33.0$ *J/cm* and $E_s = 43.0$ *J/cm* in Fig. 5.1, there exist a critical point in the space-time domain such that failure or success of the initiation process is determined. This critical point always occurs before the formation of pressure pulses that indicate the re-acceleration of the decaying shock. Instead of the address of re-accelerating mechanism, Eckett et al. [11] proposed a new approach that simply compared the magnitude of various terms in temperature reaction zone equation as selecting the failed initiation process. To follow this approach, it is necessary to extract the Lagrangian particle path data from the CFD solution.

Fig. 5.5 shows the paths of ten particles that cross the leading shock around the time of detonation failure and Fig. 5.6 shows the temperature as a function of time of the ten particle paths. Overall, the behavior of the particle paths within the reaction zone appears to be very similar to the results reported in [11]. After about 100 μs, the earlier fluid particle paths show deceleration and moving back toward the origin. This flow reversing phenomenon is due to the low pressure region at the origin of the computational domain. Refer to Fig. 5.2(a).

The temperature profiles are also similar to those in [11]. The earlier particles are rapidly heated up by the chemical reactions. However, for the fifth to eighth particles, the explosion time has significantly increased. The last two particles never heat up because the blast wave becomes too weak to heat up the reactant.

To examine the competing terms in the temperature reaction zone structure equation, Eq. (4.5), we rewrite the equation for the cylindrical coordinate ($j = 1$) into the following form:

$$\underbrace{hC_p\frac{DT}{Dt}}_{\text{Total}} = \underbrace{-(1-gM^2)\sum e_k W_k - \frac{c^2}{g}\sum\frac{W}{W_k}W_k}_{\text{Heatrelease}} + \underbrace{\frac{1}{R-x}w^2(U-w)}_{\text{Curvature}} + \underbrace{w\frac{dU}{dt} - w\frac{\partial w}{\partial t} + \frac{1}{r}\frac{\partial P}{\partial t}}_{\text{Unsteadiness}} \quad (5.1)$$

Along each particle path, each term in Eqn. (5.1), including the Lagrangian derivative, *DT/Dt*, is calculated by a post processing operation using the transient CFD results.

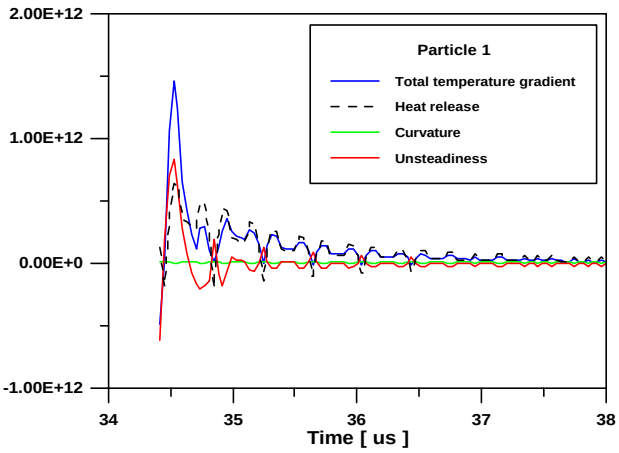


(a)

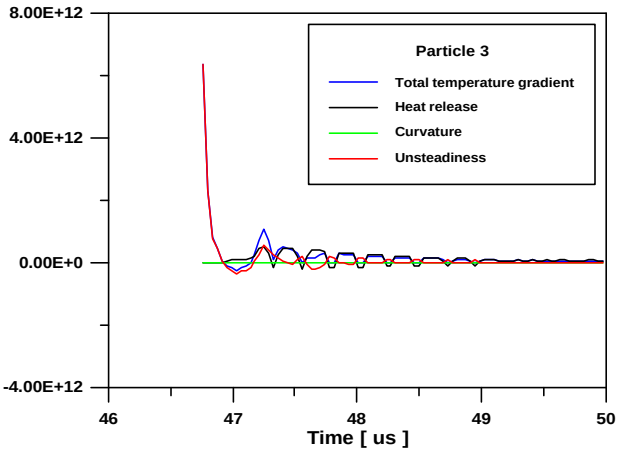


(b)

Fig. 5.7: Competing terms in (5.1) along the particle paths for $E_s = 33.9$ *J/cm*. (a) Particle 1; (b) Particle 3.

Figures 5.7(a) and (b) show magnitudes of each term in Eqn. (5.1) along two particle trajectories, before and at the failure point of the initiation process. The present results show that the effect of the curvature term contributes a little to the temperature gradient as compared to other terms. On the other hand, the effect of the unsteadiness term is significant.

## 6. CONCLUDING REMARKS

The numerical simulations of the direct initiation process of cylindrical detonation for a $H_2$-$O_2$-Ar mixture have been conducted using the space-time CESE method. Calculation has been done based on the use of realistic finite-rate chemistry models and comprehensive thermodynamics models. The three detonation initiation regimes were calculated according to the values of the deposited energy in the initial conditions, including sub-critical, critical, and supercritical. In the critical regime, the present result showed flow instabilities with strong pressure peaks. The magnitude of each term in the temperature reaction zone equation was calculated. The results of present study showed that the unsteadiness plays a critical role in impacting the Lagrangian temperature profiles along fluid particles.

## ACKNOWLEDGEMENT

We are indebted to Professor J. E. Shepherd of Cal. Tech. for the general direction of this research work. Useful interactions with other members in the ONR PDE program are also acknowledged.

## REFERENCES

1. I. B. Zel' dovich, S. M. Kogarko, and N. N. Simonov, (1956), "An experimental investigation of spherical detonation of gases," Sov. Phys. Tech. Phys. 1(8), pp. 1689-1713.
2. R. A. Strehlow and R. Cohen, (1962), "Initiation of Detonation", Phys. Fluids, Vol 5. No.1, pp. 97-101.
3. G. G. Bach, R. Knystautas, and J. H. Lee, (1969), "Direct Initiation of Spherical Detonations in Gaseous Explosives," 12th Symp. Int. Combust. Proc., pp. 853-867.
4. L. He and P. Clavin, (1994), "On the Direct Initiation of Gaseous Detonations by an Energy Source," J. Fluid Mech. 277, pp. 227-248.
5. S.-C. Chang, (1995), "The Method of Space-Time Conservation Element and Solution Element- A New Approach for Solving the Navier-Stokes and Euler Equations," Journal of Computational Physics, Vol. 119, pp.295-324.
6. L. He, (1996), "Theoretical Determination of the Critical Conditions for the Direct Initiation of Detonation in Hydrogen-Oxygen Mixtures," Combustion and Flame 104, pp. 401-418.
7. J. H. S. Lee, (1977), "Initiation of Gaseous Detonation," Ann. Rev. Phys. Chem. 28, pp.75-104.
8. K. Mazaheri, (1997), "Mechanism of the onset of detonation in blast initiation," PhD thesis, McGill University.
9. J. H. S. Lee and A. J. Higgins, (1999), "Comments on Criteria for Direct Initiation of Detonation," Phil. Trans. R. Soc. Lond., A 357, pp3503-3521.
10. S. T. Yu, S. C., Chang, P. C. E. Jorgenson, "Direct Calculation of Detonation with Multi-Step Finite-Rate Chemistry by the Space-Time Conservation Element and Solution Element Method," AIAA Paper 99-3772, AIAA 30th Fluid Dynamics Conference and Exhibit, June 1999, Norfolk, VA.
11. C. A. Eckett, J. J. Quirk, and J. E. Shepherd, (2000), "The Role of Unsteadiness in Direct Initiation of Gaseous Detonations," J. Fluid Mech. 421, pp. 147-183.
12. K.-S. Im, C.-K. Kim, and S.-T. J. Yu, "Application of the CESE Method to Detonation with Realistic Finite-Rate Chemistry," AIAA-2002-1020 the 40th Aerospace Sciences Meeting and Exhibit, January 2002, Reno, NV.